Металлофиз. новейшие технол. / Metallofiz. Noveishie Tekhnol.
2018, т. 40, № 5, сс. 625–635 / DOI: 10.15407/mfint.40.05.0625
Оттиски доступны непосредственно от издателя
Фотокопирование разрешено только
в соответствии с лицензией

PACS numbers: 61.05.cp, 62.23.Pq, 68.37.Lp, 68.65.Pq, 75.60.Ej, 75.75.Cd, 81.05.ue

Synthesis and Magnetic Characteristics of N–Co Nanocomposites

O. M. Lisova, M. V. Abramov, S. M. Makhno, and P. P. Gorbyk

O. O. Chuiko Institute of Surface Chemistry, N.A.S. of Ukraine,
17 General Naumov Str.,
UA-03164 Kyiv, Ukraine

The single-domain nanoparticles of NiCo, NiCo on the surface of graphene (NiCo@GNP) and NiCo on the surface of silica dioxide (NiCo@SiO_2) are synthesized. Their crystalline structure, surface morphology and magnetic characteristics of nanoparticle are investigated. It is shown that the magnetization curve of the nanoparticles ensembles in the form, which is distinctive for superparamagnets, and its calculations within the framework of the Langevin's paramagnetism theory are satisfactorily consistent with the experimental results. The laws of particle size distribution in ensembles are established using the method of magnetic granulometry.

Key words: nanocomposites, nanoparticles, graphene, magnetic properties, superparamagnets.

Синтезовано однодоменні наночастинки NiCo, NiCo на графеновій поверхні (NiCo@ГНП) та NiCo на поверхні діоксиду силіцію (NiCo@SiO_2). Досліджено їхні кристалічну структуру, морфологію поверхні та магнетні характеристики ансамблів наночастинок. Показано, що крива магнетованости ансамблів наночастинок має форму, характерну для суперпарамагнетиків, а її розрахунки в рамках Ланжевенової теорії парамагнетизму задовільно узгоджуються з експериментальними результатами. Методою магнетної ґранулометрії встановлено закони розподілу частинок за розмірами в ансамблях.

Ключові слова: нанокомпозити, наночастинки, графен, магнетні властивості, суперпарамагнетики.

Corresponding author: Oksana Miroslavivna Lisova
E-mail: oksana.garkusha@gmail.com

Citation: O. M. Lisova, M. V. Abramov, S. M. Makhno, and P. P. Gorbyk, Synthesis and Magnetic Characteristics of N–Co Nanocomposites, *Metallofiz. Noveishie Tekhnol.*, **40**, No. 5: 625–635 (2018), DOI: 10.15407/mfint.40.05.0625.

Синтезированы однодоменные наночастицы NiCo, NiCo на поверхности графена (NiCo@GNP) и NiCo на поверхности диоксида кремния ($NiCo@SiO_2$). Исследованы кристаллическая структура, морфология поверхности и магнитные свойства нанокомпозитов. Показано, что кривая намагниченности ансамблей наночастиц имеет форму, характерную для суперпарамагнетиков; её расчёты в рамках теории парамагнетизма удовлетворительно согласуются с экспериментальными результатами. Методом магнитной гранулометрии установлены законы распределения частиц по размерам в ансамблях.

Ключевые слова: нанокомпозиты, наночастицы, графен, магнитные свойства, суперпарамагнетики.

(Received March 1, 2018)

1. INTRODUCTION

Bimetallic nanocomposites (BNCs) containing nanoparticles (NP) of organic and inorganic materials have been attracting considerable attention of specialists in recent years [1, 2] due to a large number of possible applications [3, 4]. Prominent areas for the using of such structures are catalysis and electrocatalysis [5, 6]; in electronics, BNCs are used as electrode materials for solar and fuel cells [7, 8], electric and biosensors [9, 10], as corrosion-resistant materials and much more. The importance of searching for new methods of obtaining and researching BNCs is due to their multifunctionality, the possibility of a unique combination of the properties of many materials in one [4]. They acquire better catalytic, thermal, optical, electrical, and magnetic properties as compared to monometallic and bimetallic particles without a matrix. Consequently, the presence of a matrix not only plays the role of a substrate, but also is a functionally active element [11]. Composites are obtained on various inorganic (kaolin, zeolites and zirconium) and organic (artificial and natural polymers, graphite derivatives) matrices [1, 6, 12].

In recent years, various methods for obtaining bimetallic BNCs have been developed, the synthesis of which is carried out by spraying methods [13, 14], glow discharge [15], pulsed laser ablation [16], reversed micelles [17], thermal decomposition [18], chemical recovery from a solution [19, 20]. Most often, bimetallic LFs are obtained by simultaneous restoration of two metal ions in conditions of stabilization of the chemical composition, size, and shape of particles. BNCs have different forms; they exist in the form of alloys or contact agglomerates, such as kernel–shell, *etc*.

Particular attention is paid to the magnetic properties of BNCs containing ferromagnetic NPs on carbon-containing matrices, which are investigated for creating water-purifying filters [21, 22], rechargeable

batteries, various sensors [4], protective materials from corrosion and deterioration [11] and electromagnetic waves [23] and others.

The purpose of the work is to study the structural and magnetic properties of ferromagnetic nanoparticles NiCo, NiCo@GNP and NiCo@SiO_2 nanocomposites.

2. MATERIALS AND METHODS

Graphene nanoplates (GNP) are obtained by electrochemical deposition in an electrolyte (KOH) of a low concentration at a current passing to 60 mA/cm^2. Electrodes were placed between polypropylene fabric filters for the separation of large graphite particles from nanosized ones. GNPs are stored in the form of a suspension with a mass concentration of graphene 2% and pH = 12. The NiCo particles were obtained by the method of chemical precipitation from a solution of hydrazine hydrate of nickel and cobalt carbonates [24] at a temperature of 350 K. The technique was modified for the purpose of synthesis of NiCo@GNP composites, coprecipitation of a solution of carbonates and a suspension of graphene was prepared at a boiling point of hydrazine hydride at a mass ratio of 9:1 components. The presence of KOH in a suspension of graphene created favourable conditions for the synthesis of metal particles. GNPs play the role of crystallization centres as well as contribute to the stabilization of the size and chemical composition of nanoparticles.

For the synthesis of NiCo@SiO_2 composites, a SiO_2 suspension had been previously prepared by mixing tetraethoxysilane with ethyl alcohol and ammonium hydroxide in a ratio of 1:20:10. The slurry was added to a Ni and Co carbonates solution in hydrazine hydrate.

X-ray diffraction analysis was performed by powder diffractometry on a DRON-4-07 diffractometer while the emission of an anode line CuK_α with a nickel filter in the reflected beam at the geometry of the Breguet–Bretagne shooting. The morphology of the specimens was studied using a JEOL JEM-1230 transmitted electronic microscope.

The hinges of the magnetic moment of the specimens were measured using a laboratory vibration magnetometer at a room temperature. The description of the installation and the method of measurement are described in [25]. Specially prepared, demagnetized specimens were measured. For comparison, a test sample of nickel was used. The measurement error of the specific saturation magnetization (σ_s) relative to the tested sample did not exceed $\pm 2.5\%$.

3. RESULTS AND DISCUSSION

The electron-microscopy studies revealed the presence of nanometer-size particles in all three understudied systems. It is shown that, on the

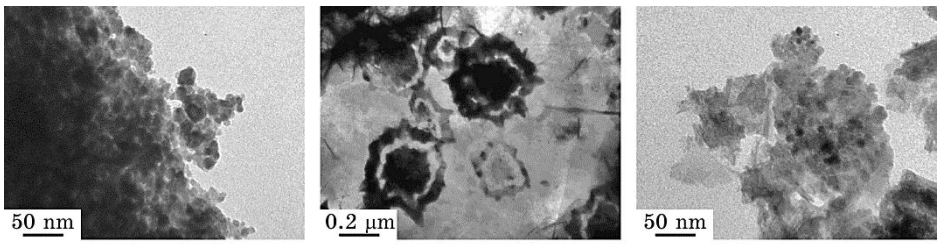

Fig. 1. PEM images of the NiCo (*a*), NiCo@GPN (*b*), NiCo@SiO_2 (*c*) NP.

surface of the GNP, there are metal particles in the size range ≅ 20–200 nm (Fig. 1, *b*); in more detailed images of graphene film, metal particles of 20 nm can be observed. Large particles are probable to be agglomerates consisting of small ones [24].

The results of the x-ray diffraction (Fig. 2) analysis indicated the presence of phases of GNP, nickel, cobalt and the absence of reflexes of the incoming carbonates. Thus, peaks of 22.4° and 31.3° can be related to the presence of graphene structures in samples, and a low-intensity band of 27.1° corresponds to a crystalline lattice of graphite. Particles of nickel may correspond to peaks of 44.9°—octahedral (111), 52.2° and 91.8°—cubic syngony.

The cobalt crystalline lattice of a cubic syngony corresponds to peaks of 52.2° (111), 61.2° (200), 91.8° (220), hexagonal—55.9° (101). Consequently, the peaks of 52.2° and 91.8° may indicate the presence of bime-

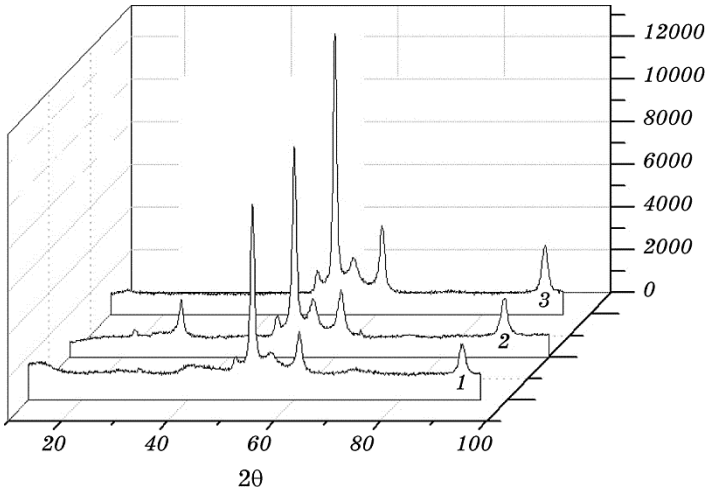

Fig. 2. The diffraction pattern of the NiCo (*1*), NiCo@GNP (*2*) and NiCo@SiO_2 (*3*) samples.

TABLE 1. Statistical parameters of low-frequency NiCo and NiCo@GNP, NiCo@SiO_2 structures.

Pattern	N	$\langle D\rangle$, nm	σ_D, nm	$\langle \ln D\rangle$	$\sigma_{\ln D}$
NiCo	62	9.96991	3.71358	2.24052	0.34173
NiCo@ГНП	63	23.33829	8.84181	3.08827	0.34629
NiCo@SiO_2	64	8.67567	3.36113	2.08959	0.38353

N—the amount of particles, $\langle D\rangle$—the average of the NP diameter, σ_D—the standard deviation of the NP diameter, $\langle \ln D\rangle$—the average of the logarithm of the NP diameter, $\sigma_{\ln D}$—standard deviation of the logarithm of the NP diameter.

tallic particles of NiCo with a cubic crystal lattice (200) [13]. The size of crystallites, calculated by Scherrer's equation, is 15–20 nm.

The parameters of the basal cell NiCo and NiCo@GNP and NiCo@SiO_2 bands obtained by statistical processing of the PEM images of the corresponding samples are given in Table 1.

The size distribution of superparamagnetic particles can be determined by measuring the magnetization curve $M(H)$, pronounced by the Langevin function [26], we assume that all particles have a spherical shape without interaction.

The normal distribution is determined by the Gauss equation:

$$p(d, M_d, \sigma_d) = \frac{1}{\sigma_d \sqrt{2\pi}} e^{-\frac{(d-M_d)^2}{2\sigma_d^2}}, \quad (1)$$

where M_d and σ_d are expected value and standard deviation of the NP diameter, respectively.

The lognormal distribution of particles in diameters is determined by the equation:

$$p(\ln d, M_{\ln d}, \sigma_{\ln d}) = \frac{1}{d\sigma_{\ln d} \sqrt{2\pi}} e^{-\frac{(\ln d - M_{\ln d})^2}{2\sigma_{\ln d}^2}}, \quad (2)$$

where $M_{\ln d}$ and $\sigma_{\ln d}$ are expected value and standard deviation of the logarithm of the NP diameter, respectively.

With the use of an experimental distribution in size, one can predict the density of a normal or lognormal distribution. With a particle amount more than 50, the probability density with the accuracy of the experiment corresponds to the general population, which means a sufficient statistical sampling. Figures 3–5, *a* show the experimental distribution of the diameters of the three NiCo, NiCo@GNP and NiCo@SiO_2 systems. NiCo@SiO_2 and NiCo@GNP systems have a more even distribution, albeit they are significantly different from the val-

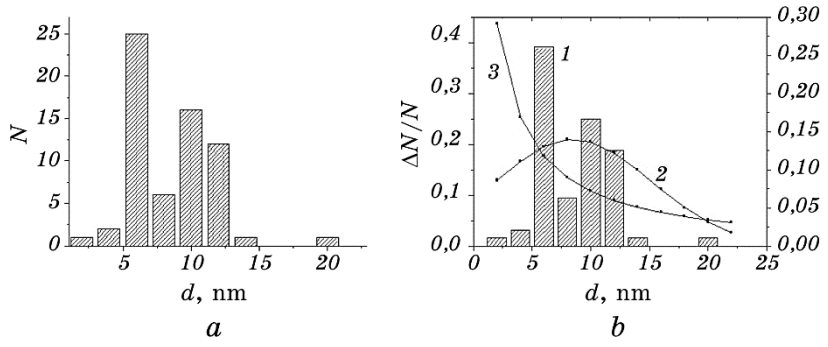

Fig. 3. *a*—the NP distribution by the diameters for the NiCo system; *b*—the polygon of the relative frequencies of the NP diameters, and the probability density calculated by the lognormal distribution *1* by Eq. (1) of the NP ensemble of NiCo particles and by the normal distribution *2* by Eq. (2).

ues of the largest and smallest bore diameters.

Curves obtained in Fig. 3–5, *b* show that the NiCo particles are distributed by diameters closer to the normal distribution, the maximum values of NiCo@GNP are closer to the lognormal, and NiCo@SiO_2 in accordance with the normal. An analysis of form of the distribution of nanoparticles can serve as a means for testing hypotheses regarding the nature of their growth in the process of chemical condensation [30]. In most cases, formation of a low frequency is followed by two processes: sequential and/or parallel growth. In the case of the random nature of the interactions between the NP, with the parallel growth (without interaction between the crystals), it is likely that the distribution of the NP in size is normal (Gaussian), while in the sequential manner, it is lognormal [31].

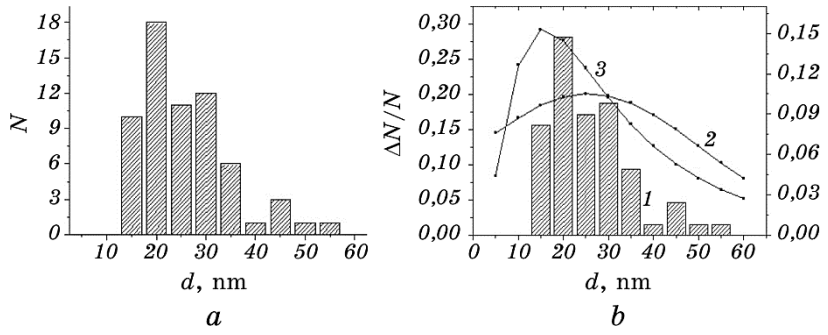

Fig. 4. *a*—the distribution by diameters, *b*—the polygon of relative frequencies of diameters and density of probability calculated by Eq. (1) for the NP ensemble of NiCo @ GNP (N = 63): *1*—lognormal, *2*—normal distribution of the NiCo bulk and NiCo nanoparticles in the NiCo@GNP nanocomposite.

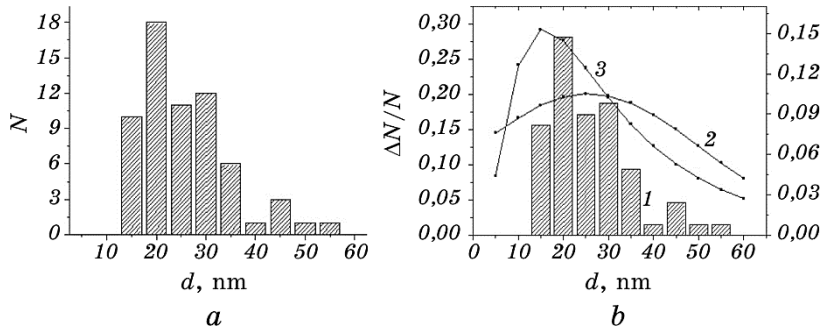

Fig. 5. *a*—the distribution by diameters, *b*—the polygon of relative frequencies of diameters and density of probability calculated by Eq. (1) of the Ni-Co@SiO_2 NP ensemble ($N = 64$). *1*—lognormal, *2*—normal distribution of the NiCo bulk and NiCo@SiO_2 nanocomposite.

For the system of magnetosensitive SiO_2/Fe_3O_4 nanocomposites, it was shown [25, 32] that artificial nucleation can produce magnetic material with an average crystallite size of 5–8 nm and a value of a specific surface area that is 2–3 times higher than the corresponding value for magnetite obtained by the Elmor's method.

Stabilization of magnetic NP on primary particles can increase the stability of nanocomposite system particles. NiCo fixed on the surface of SiO_2 and GNP or incorporated into the space between these particles have spatial barriers to aggregation among themselves, but remain accessible to other reagents of the existing system. It is important that they can not only store their basic physical and chemical characteristics, but also acquire new ones.

By the method of magnetic granulometry [27], which is based on the comparison of the experimental and Langevin magnetization curves with given laws of particle-size distribution and their magnetic parameters, in particular, the magnetization of saturation of the particle material and the thickness of degaussed layer, according to the experimental magnetization curve of the NSC, they were found to be in the size distribution of the NP. For the analysis of magnetization curves, the known equation [28, 29]

$$\frac{\sigma^{NCP}(H)}{\sigma_s^{NCP}} = \left(\sum_{i=1}^{k} n_i D_i^3 \right)^{-1} \sum_{i=1}^{k} n_i (D_i - 2\varepsilon)^3 L\left(\frac{M_s^{\text{bulk}} H}{k_B T} \frac{\pi}{6} (D_i - 2\varepsilon)^3 \right), \qquad (3)$$

where $\sigma^{NCP}(H)$, σ_s^{NCP} —the NP specific magnetization in the applied field of intensity H and the specific magnetization of the NP saturation, respectively, M_s^{bulk} —the magnetization of the saturation of the massive nickel crystal; D_i, n_i—the mean diameter and the number of NP in the i-th range of the variational row of diameters; k—number of

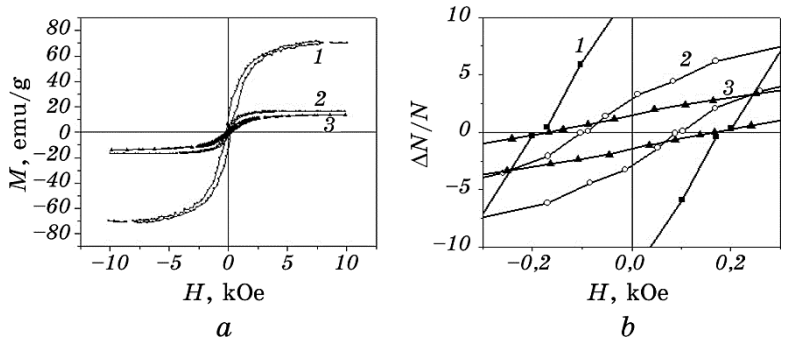

Fig. 6. Loops of hysteresis (*a*) of the NiCo (*1*), NiCo@GNP (*2*), NiCo@SiO_2 (*3*) samples; the central part of the hysteresis (*b*).

intervals; ε—the thickness of the surface NP with nonlinear magnetic moments; $L(\xi) \equiv \mathrm{cth}\xi - 1/\xi$—Langevin function; k_B—Boltzmann constant; T—absolute temperature.

In Figure 6, it is evident that the magnetization of NiCo@GNP and NiCo@SiO_2 samples is similar in the application of magnetic field of 10 kOe. The magnetization of a NiCo sample is much higher in the magnetization of composite specimens, which, assuming the same low-frequency size for the NiCo@SiO_2 system, indicates the content of the nonmagnetic component of the NP in the composite.

Saturation magnetization depends on the size of particles. The ratio of saturation magnetization (Table 2) for the NiCo and NiCo@SiO_2 samples (exactly these samples can be compared, since they have approximately the same particle sizes), σ_s(NiCo@SiO_2)/σ_s(NiCo), is about 24% (by mass) of magnetic nanoparticles in the NiCo@SiO_2 composite. For larger NiCo@GNP particles, a comparison with literature data [33] shows that the mass fraction of magnetic particles is about 20%.

The residual magnetization of the NiCo@SiO_2 sample (Fig. 6, *b*) is twice as low as the NiCo nanoparticles output, and is twice as low as the coercive force, so the NiCo@SiO_2 particles are more easily magnetized than the NiCo NP. The above-mentioned characteristics describe the ensemble of particles, not each separately.

TABLE 2. Magnetic characteristics of the NiCo and BNC nanoparticles on their basis.

Pattern	H_c, Oe	σ (10 kOe), Gs·cm^3/g	σ_s, Gs·cm^3/g
NiCo	178 (± 1%)	71.1 (± 2.5%)	73.2 (± 2.5%)
NiCo@ГНП	164 (± 1%)	13.8 (± 2.5%)	14.2 (± 2.5%)
NiCo@SiO_2	91 (± 1%)	16.8 (± 2.5%)	17.3 (± 2.5%)

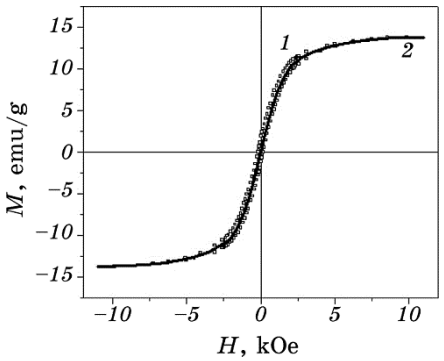

Fig. 7. *1*—the hysteresis loop of the NiCo@GNP sample obtained experimentally, *2*—the theoretical curve obtained by Eq. (4) for the low NiCo@GNP ($N = 63$) with parameters $M_{\ln V} = 8.61774$ and $\sigma_{\ln V} = 1.03888$.

In one-domain state, the prevailing mechanism of reversal is a process of coherent rotation of magnetic moments, which is hindered by crystallographic anisotropy and anisotropy of form of a particle. The maximum coercive force of reversal of the ensemble of chaotically oriented noninteracting particles with uniaxial anisotropy can be represented as two terms (neglecting the anisotropy of mechanical stresses):

$$H_c = {}_K H_c + {}_N H_c = 0.64\, K/I_s + 0.479(N_a - N_R)I_s, \tag{4}$$

where ${}_K H_c$, ${}_N H_c$ are maximum value of the reciprocal field caused by the presence of crystallographic anisotropy and the component caused by the anisotropy of form [32], respectively; K is the anisotropy constant.

In approximation of a spherical particle, $N_a - N_R$, the second term of Eq. (4), turns to zero. An analysis of the hysteresis loops of composites taking into account Eq. (4) indicates the possibility of determining the value of the constant of the crystallographic anisotropy of the NiCo NP, which characterizes an ability of the material to remagnetization.

$$I_s = \rho\sigma_s, \tag{5}$$

where ρ is the density of the material, σ_s is the specific magnetization of saturation, from where $K = H\rho\sigma_s$, $K = 1.8 \cdot 10^5$ erg/cm^3. The constants of anisotropy for Ni and Co are equal to $-0.5 \cdot 10^5$ erg/cm^3 and $45 \cdot 10^5$ erg/cm^3 [33], respectively. Therefore, the calculated value is within the specified limits.

4. CONCLUSIONS

The NiCo, NiCo on the surface of graphene (NiCo@GNP) and NiCo on

the surface of silica dioxide ($NiCo@SiO_2$) nanoparticles were obtained by chemical precipitation from a solution of hydrazine hydride. The conducted PEM and x-ray studies showed the presence of phases of nanometer-size composites.

The crystallographic anisotropy constant for the NiCo nanoparticles and the mass content of magnetic nanoparticles in the $NiCo@SiO_2$ and NiCo@GNP composites are equal to 24 and 20% , respectively.

The method of magnetic granulometry has established that the NiCo and $NiCo@SiO_2$ particles have a normal size distribution, and NiCo@GNP is lognormal, which indicates a different mechanism of growth. For NiCo and $NiCo@SiO_2$, a parallel crystal growth is typical, and for NiCo@GNP, successively due to the influence of surface of a matrix. Study of the distribution of size of synthesized particles shows that the nature of growth of crystals can be controlled changeably.

REFERENCES

1. G. Sharma, M. Naushad, A. Kumar, S. Devi, and M. R. Khan, *Iran. Polym. J.*, **24**: 1003 (2015).
2. G. Sharma, D. Kumar, A. Kumar, A. H. Al-Muhtaseb, D. Pathania, M. Naushad, and G. T. Mola, *Mater. Sci. Eng. C*, **71**: 1216 (2017).
3. G. Sharma, A. Kumar, Sh. Sharma, Mu. Naushad, R. P. Dwivedi, Z. A. ALOthman, and G. T. Mola, *Journal of King Saud University – Science* (2017).
4. S. M. Hamidi, B. Mosaeii, M. Afsharnia, A. Aftabi, and M. Najafi, *J. Magn. Magn. Mater.*, **417**: 130 (2016).
5. Y. Han, W. Li, M. Zhang, and K. Tao, *Chemosphere*, **72**: 53 (2008).
6. B. Habibi and S. Ghaderi, *Int. J. Hydrogen Energy*, **40**, Iss. 15: 5115 (2015).
7. M. Motlak, N. A. Barakat, M. S. Akhtar, A. M. Hamza, B. Kim, C. Sang, K. Abdelrazek, and A. A. Almajid, *Electrochim. Acta*, **160**: 138 (2015).
8. V. Dao, Y. Choi, K. Yong, L. L. Larina, O. Shevaleevskiy, and H. Choi, *J. Power Sources*, **274**: 831 (2015).
9. M. Cui, J. Huang, Y. Wang, Y. Wu, and X. Luo, *Biosens. Bioelectron.*, **68**: 563 (2015).
10. C. Kung, P. Lin, F. John, Y. Xue, and X. Yu, *Biosens. Bioelectron.*, **52**: 1 (2014).
11. S. Awasthi, S. K. Pandey, A. Juyal, C. P. Pandey, and K. Balani, *J. Alloys Compd.*, **711**: 15 (2017).
12. R. Ahmad, A. S. Qureshi, L. Li, J. Bao, X. Jia, Y. Xu, and X. Guo, *Colloids Surf. B: Biointerfaces*, **143**: 490 (2016).
13. S. Akamaru, M. Inoue, Y. Honda, A. Taguchi, and T. Abe, *Jpn. J. Appl. Phys.*, **51**, No. 6R: 065201 (2012).
14. M. Maicas, M. Sanz, H. Cui, C. Aroca, and P. Sánchez, *J. Magn. Magn. Mater.*, **322**: 3485 (2010).
15. G. Saito, S. Hosokai, T. Akiyama, S. Yoshida, S. Yatsu, and S. Watanabe, *J. Phys. Soc. Jpn.*, **79**: 083710 (2010).
16. P. Kalita, J. Singh, M. K. Singh, P. R. Solanki, G. Sumana, and B. D. Malhotra, *Appl. Phys. Lett.*, **100**: 093702 (2012).

17. P. Calandra, *Mater. Lett.*, **63**: 2416 (2009).
18. I. Gonzalez, J. C. De Jesus, E. Cañizales, B. Delgado, and C. Urbina, *J. Phys. Chem. C*, **116**: 21577 (2012).
19. T. Bala, R. D. Gunning, M. Venkatesan, J. F. Godsell, S. Roy, and K. M. Ryan, *Nanotechnology*, **20**: 415603 (2009).
20. Y. Yamauchi, T. Itagaki, T. Yokoshima, and K. Kuroda, *Dalton Trans.*, **41**: 1210 (2012).
21. X. Wu, Z. Zhang, C. Xia, B. Chen, and X. Min, *J. Alloys Compd.*, **718**: 15 (2017).
22. E. Motamedi, M. Talebi Atouei, and M. Z. Kassaee, *Materials Research Bulletin*, **54**: 34 (2014).
23. X. Lv, J. Guo, C. Zhao, Y. Wei, J. Zhang, Z. Wu, and C. Gong, *Mater. Lett.*, **201**: 43 (2017).
24. P. V. Lapsina, *Nanostrukturirovanye Poroshki Ni, Co i Sistemy Ni–Co, Poluchenhye Vosstanovleniem Kristallicheskikh Karbonatov Vodnym Rastvorom Gidrazin Gidrata* [Nanostructured Powder of Ni, Co and Ni–Co System Obtained by Recovery of Crystalline Carbonates by Water Hydrazine Hydrate Solution] (Thesis of Disser. for Dr. Chem. Sci.) (Kemerovo: 2013) (in Russian).
25. M. V. Borysenko, V. M. Bogatyrov, I. V. Dubrovin, M. V. Abramov, M. V. Gayevaya, and P. P. Gorbik, *Fiziko-Khimiya Nanomaterialov i Supramolekulyarnykh Struktur* [Physicochemistry of Nanomaterials and Supramolecular Structures] (Kiev:2007) (in Russian).
26. C. P. Bean and J. D. Livingston, *J. Appl. Phys.*, **30**: 120S (1959).
27. A. Yu. Olenin, *Rossiyskie Nanotekhnologii*, **7**, Nos. 5–6: 53 (2012) (in Russian).
28. M. M. Labushev, *Matematicheskie Metody i Modeli pri Reshenii Geologicheskikh Zadach na EhVM* [The Mathematical Methods and Models for Solving Geological Problems on a Computer] (Krasnoyarsk: 2007) (in Russian)
29. V. M. Bogatyrov, M. V. Borysenko, I. V. Dubrovin, M. V. Abramov, M. V. Galaburda, and P. P. Gorbyk, *Nanomaterials and Supramolecular Structures : Physics, Chemistry, and Applications* (Eds. A. P. Shpak and P. P. Gorbyk) (Dordrecht,Netherlands: Springer: 2009), p. 159.
30. C. P. Bean and I. S. Jacobs, *J. Appl. Phys.*, **27**: 1448 (1956).
31. R. Kaiser and G. Miscolczy, *J. Appl. Phys.*, **41**, No. 3: 1064 (1970).
32. E. E. Bibik, B. Ya. Matyrgulin, Yu. L. Raykher, and M. I. Shliomis, *Magnitnaya Gidrodinamika*, **68**, No. 1: 68 (1973) (in Russian).
33. B. D. Cullity and C. D. Graham, *Introduction to Magnetic Materials* (Wiley-IEEE Press: 2009).